

A 3D Numerical Reservoir Model for Steamboat, Nevada

Grimur Bjornsson¹, Andri Arnaldsson², and John Akerley³

¹Reykjavik Geothermal

²Vatnaskil Consulting Engineers

³Ormat Technologies, Inc.

Keywords

Reservoir modeling, iTOUGH2, resource management, case study, Steamboat, Nevada, Ormat

ABSTRACT

The Steamboat project in South-Reno, Nevada, is among the most successful and long standing geothermal power projects in the US. Despite its shallow average well depth and very short distance between production and injection sectors, the reservoir is responding to the twenty-five years of massive flow with a negligible pressure drawdown and moderate cooling rates compared to other geothermal locations worldwide.

The greater than 130 Steamboat wells drilled, large volume of downhole and production data, and structural information gathered comprise ideal circumstances for developing a high resolution numerical model. Additionally, advances in inverse modeling technology and rapidly increasing computer power move the task of modeling Steamboat from a forward model nightmare to a complex but rewarding inverse modeling exercise. The 20x40 km mesh area now developed is split into 14 layers of 2.5 km total thickness. About 40 thousand elements provided a sufficiently detailed mesh to capture the field data at hand, and 1270 datasets were calibrated against by the inverse technology. The deep and outer model elements are of less than 5 mD permeability and fracture zones are of several hundred mD while the shallow lower Steamboat permeability is as high as 10 Darcys. The model is heated by a deep 95 kg/s recharge of 236-250°C. A cold recharge occurs from the NW into the shallow model, imitating the hydraulic head of the Sierra mountain range. Around 160 kg/s exit the shallow model to the north as natural discharge into the Truckee Meadows alluvium and to the naturally occurring hot springs. Of this mass flow, two thirds are modeled as from the deep upflow and one third is outer boundary recharge.

Systematic analysis of the calibrated model, assisted by splitting the reservoir into sectors and focusing on usable heat (>100 °C), shows that the Lower Steamboat sector has and will continue

to sustain a large proportion of the early and current power production, later supplemented by heat and mass from the much hotter and deeper Steamboat Hills wells. As the heat reserve of Lower Steamboat is drained, the model is suggesting more dispersed injection and increased mass production from the Steamboat Hills wells as appropriate resource management strategy.

Introduction

With a maturing worldwide geothermal industry, many developers have shifted their attention from green field exploration and early power plant commissioning to stabilizing existing power projects and preferably maximizing their output at reasonable cost. One tool that assists developers in achieving such a level of resource management is numerical modeling. These models are capable of incorporating the large volume of field data at hand. They also can account for variability in the resource history, including wells going on and off line, impact of injection sectors, both temperature and pressure changes with time, and tracer data to better understand the reservoir volume connecting injection and production wells. Finally, when production histories exceed 10-20 years, the numerical models are able to shed light on the wellfield outer boundaries and in particular the natural recharge coming in to replenish some of the mass and heat being removed by production.

This paper demonstrates a complex reservoir model recently calibrated on Steamboat. After introducing the conceptual reservoir model, the model mesh is explained. Then the inverse modeling process is addressed along with what datasets were introduced to constrain the model parameters. The model match to the initial temperature and pressure data is shown, followed by comprehensive study on the reservoir temperature changes with time. The concept of usable heat is then introduced and shows how breaking the reservoir into sectors between south and north can greatly simplify analysis on the field response to production and injection. The paper ends with conclusions, including which resource management options may best maintain power production from this impressive resource.

Setting up a Complex Numerical Model

The Steamboat project of Ormat is amongst the most complex reservoir models being calibrated by the authors of this paper. This reservoir incorporates over 130 wells drilled, tens of years of production and injection history cumulating at 3 tons per second each, reservoir sectors that either respond as matrix or fracture dominated media to production and, furthermore, has a strong magmatic component in its upflow area. With that said, other complexities accompany the field operating history like changing ownership of power plants and production sectors and field data scattered between paper copies at the early stage to now modern high density data-logging.

Calibrating numerical models to match such a large dataset is therefore a major effort that needs good preparation and the right tools and computer environment. Firstly, a properly calibrated model should match all field data at hand that affect heat and mass balance at depth. Secondly, such a model may need a large number of elements to properly incorporate the various geological features that arise from years of drilling and exploration. Combined, these two features will result in the need for sizeable computing power and a numerical model setup that easily hosts the field data at hand and is capable of writing out and plotting the large number of datasets.

The authors of this paper have nearly 15 years of modeling experience and cooperation on Ormat projects, in the process delivering a sizeable volume of both new and recalibrated numerical models on fields between Africa and the Americas. A key success element in this work was the introduction of inverse modeling and parallel computing on Linux clusters. The simulator has always been iTOUGH2 (Finsterle 2007), allowing for ease in specifying the data at hand and ensuring it supports the model as expected in the right coordinates and at the right time of being collected. The shell script culture of Linux and graphical interfaces like the Generic Mapping Tool (Wessel 2013), various homemade Fortran, C and Perl codes and a relational database play important roles in allowing the modelers to focus on the model instead of the computer. Finally the modelers are in the process of finalizing a mesh pre- and postprocessor that greatly assists in developing and maintaining the model mesh.

Conceptual Reservoir Model

The Steamboat conceptual reservoir model used as basis for the current numerical model comes initially from the large number of open source papers accessible from the IGA website and elsewhere (Thompson and White 1964, White et al. 1964, White 1968, Desormier 1984, Skalbeck et al. 2002, Yankee-Caithness 2002, Walsh et al. 2010). Through calibrating the numerical model, however, the conceptual model had at times to be revisited and slightly revised.

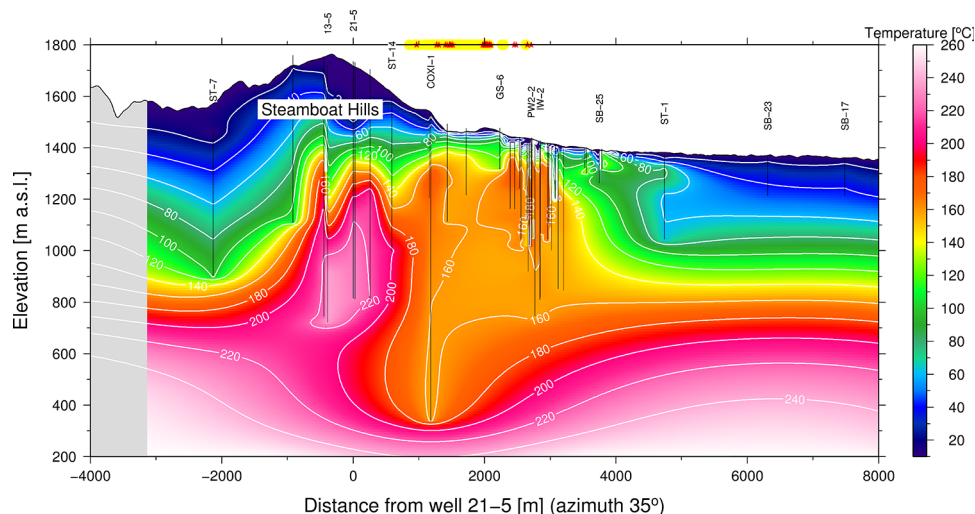


Figure 1. Temperature in a N35E cross-section across Steamboat as of 1987, with well tracks shown as lines and warm spring and fumarole locations near the cross section are shown in yellow and red, respectively.

The Steamboat reservoir differs from many other Nevada basin range systems by having a strong magmatic component (Silberman et al. 1979, Arehart et al. 2003). The recent volcanism may thereby both serve as a deep heat source for the reservoir but also has generated secondary mineralization that affects permeability of the formation overlying the upflow zone.

Figure 1 shows temperature contours of a N35E striking section as determined by estimated formation temperatures for each well. This analysis suggests the hottest upflow zone is to the south of the current wellfield. The hot water ascends to about 1200-1300 m elevation where it flows laterally to the NE before being discharged to the surface or the Truckee Meadows alluvium, which occupies the topmost 300 m of the NE part of Figure 1 cross section. Also seen in the figure is a gentle temperature reversal at approximately 900-1100 m elevation under the center and north wellfield. This infers that in the natural state, the Steamboat reservoir hosted a convective cell. Within it, water was drawn from the north at depth, mixed with the hot upflow fluid to the south and eventually rose again towards the surface. Note also that at the top margin of Figure 1, warm spring and fumarole locations near the cross section are shown in yellow and red, respectively. This mass loss removed part of the cycling water and additionally geothermal fluid was lost towards the north into the alluvium.

Dominant fault and lineament directions within the Ormat concession are between N and NE in compliance with the thermal anomaly shown in Figure 1. Several other NE trending structures are present to the west of the concession. Thirdly, WNW trending fault structures have been proposed under the Steamboat Hills, explaining correlation of well feedzones there. These structures are dominantly steeply-dipping, normal or strike-slip faults of which many are found to be exceptionally permeable when intersected by wells (Yankee-Caithness 2002). In the hottest upflow region in the SW, measured well temperatures have exceeded 240 °C. The matrix formation between the faults is tight, inferring that production from the deep faults is strongly dependent on recharge from other sectors of the resource.

Figure 2 shows the basic components of the Steamboat conceptual model. In the deeper reservoir, dominant fault strike is to

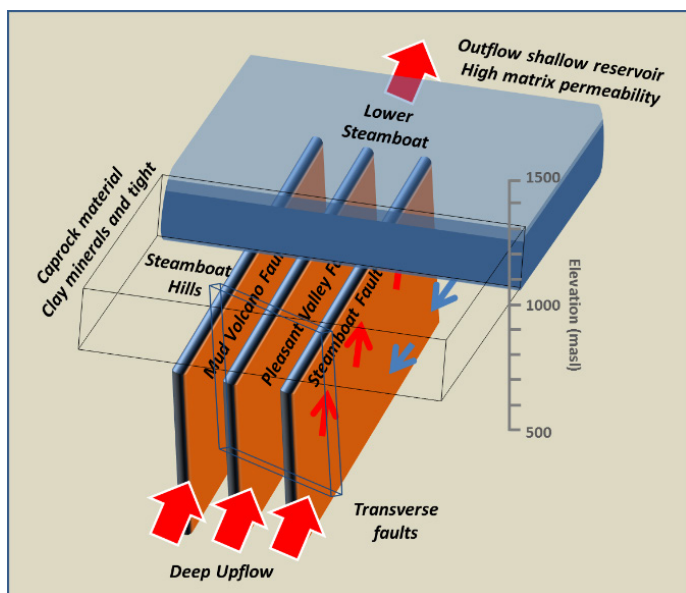


Figure 2. Schematic of the Steamboat conceptual model.

the NE. Three major structures are identified as the Mud Volcano, Pleasant Valley and Steamboat faults, with at least one fault zone under Steamboat Hills, not named, transverse to these (Walsh et al. 2010). The shallow formation overlying the principal NW faults under Steamboat Hills appears very tight as reflected in linear gradient temperatures in the shallow strata. This is seen in well surveys where the formation temperature changes from conductive to convective at about 1000 m elevation. Precipitation of clay minerals is considered as a driving mechanism for this sealing, originating from the approximately 240 °C high temperature convection cell at depth.

The Lower Steamboat shallow stratum is on the other hand behaving as exceptionally permeable, possibly a combination of tectonic action and being an alluvial formation of very good intrinsic matrix permeability. As previous studies have excluded shallow outflow into the alluvium layers to the north of Lower Steamboat (Skalbeck 2001), the only remaining option for the injected water to flow is vertically down. This proved to be fundamentally important in explaining the outstanding performance of the small Steamboat wellfield with time.

Model Mesh

Several special features of the wellfield had to be accounted for in the model mesh. As some of the fault structures are still inferred rather than confirmed, the mesh needed to allow for flexibility in fine tuning the fault locations by only changing the element rock property but not the mesh geometry. A simple but robust approach was chosen to satisfy the above. First, the model mesh is defined as large: 20x40 km and oriented to the NNE. The south and west model boundaries correspond to the Carson Range and the Sierras, while the NE boundary is the northern outskirts of Reno and Truckee Meadows. Second, a high density hexagonal element configuration is defined in the center model, roughly corresponding to the reservoir volume bounded by the Mud Volcano fault in the west, and the Steamboat fault to the East, as seen in Figure 2.

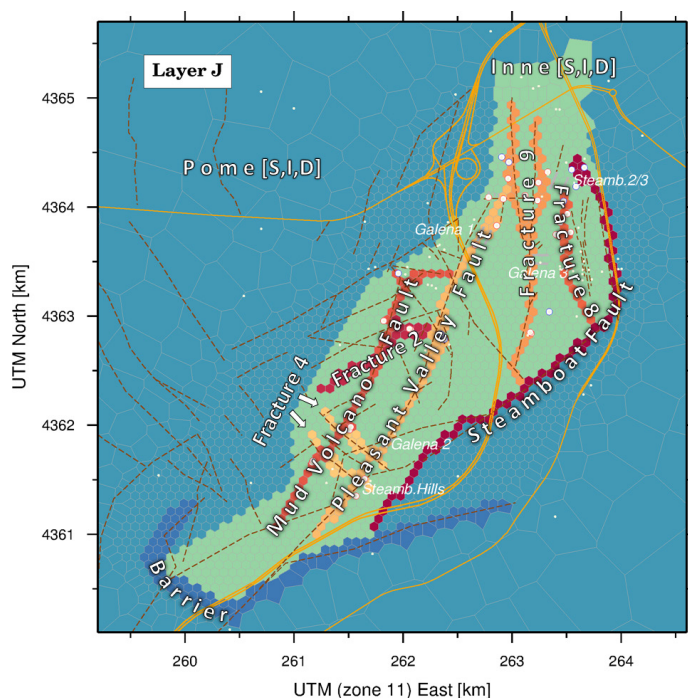


Figure 3. The inner wellfield mesh in Layer J.

The currently under development “Steinar” mesh maker of Vatnaskil proved to be of substantial help in developing a 3-D numerical model of the scale and complexity of Steamboat. A special feature of the software conveniently generated the hexagon style regular mesh inside a mouse click specified polygon. The hexagon elements are roughly 70 m across within the inner mesh. All the other model layers are identical in size and element shape while thickness is variable, as is, of course, the rocks assigned to each of them. The larger model mesh is dictated by some of the preferences and taste of the authors. For example, pushing the outer model boundaries far away and assigning them a linear temperature gradient as seen in Spampinato et al. 2010. The outermost rim elements in all layers but the top and base are given a rock property of infinite heat capacity to define it as a constant temperature boundary but not necessarily pressure. For minimizing the number of model elements, the outer elements are large and rectangular, and moving into the wellfield the mesh gets much tighter.

Figure 3 shows the center model mesh at Layer J, about 2500' elevation (650 m model depth or 750 m a.s.l.). The figure summarizes many of the principal model features. Roads are shown in orange, all wells by small white dots, production wells with larger red dots with white rim, and the injection wells are shown by blue dots with white rim. The rock material is defined next to the faults as Inne [S,I,D] where S, I and D refer to shallow, intermediate and deep, respectively. Similarly, the outer model volumes have a name prefix Pome with the same shallow, intermediate and deep notation. The figure also shows by element colors how the individual fault locations are imitated in the model mesh, and their name is placed on top. Several of the faults named in Figure 3 are also shown schematically in the conceptual reservoir model in Figure 2. Most prominent are the NE striking Mud Volcano, Pleasant Valley and Steamboat faults. Splaying out from these are unnamed fractures, shown

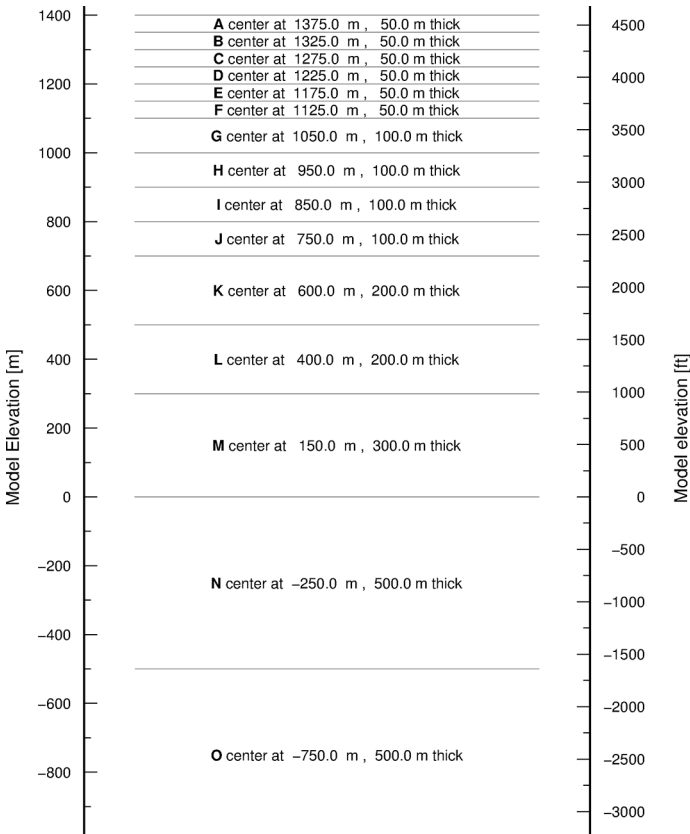


Figure 4. Vertical layering of the numerical model mesh.

with brown, dashed lines. Finally, a barrier surrounds the south wellfield.

The vertical stacking of the fifteen Steamboat numerical model layers being defined here is shown in Figure 4. A basic strategy in selecting the layer thicknesses came from the Steamboat well family.

A histogram of the bottomhole elevations and drilled depths is shown in Figure 5. The figure shows the generally shallow completion of the Steamboat wells; with wells exceeding 1000 m drilled depth virtually nonexistent. The analysis on feedzone locations, shown in Figure 6, also infers that most wells are drilled into a loss and then just some tens of feet more for a TD. The left hand side of Figure 5 was used to specify a sequence of only 50

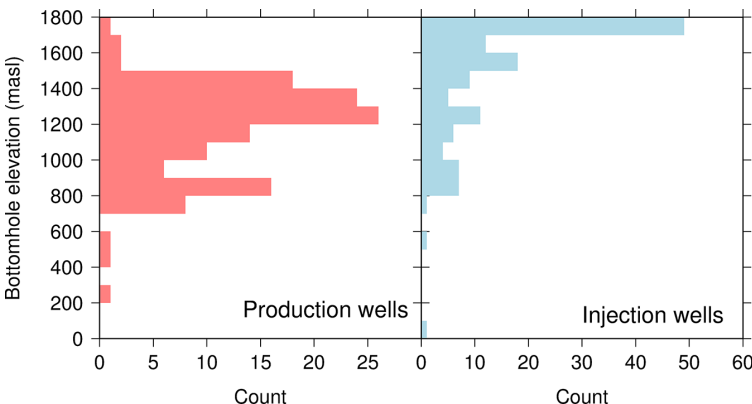


Figure 5. Histogram of Steamboat bottomhole elevations and drilled depths.

m thick model layers from 1400 m elevation to 1100, where the layer thickness is raised to 100 m. Finally, below 700 m depth the model layers get even thicker in line with lack of well data to calibrate against. The model was nevertheless extended to about twice the deepest wells to allow for deep vertical convection in the model calibration.

The short distances between injection and production wells in Steamboat, but gentle cooling rates, initially required a model mesh considerably thicker than shown in Figure 4. This was to allow for deep vertical convection and large conductive heat exchange surfaces of permeable faults and the adjacent relatively tight matrix. However, this set up led to an unstable hydrostatic pressure gradient and, at times, very large invasion of cold fluid from the north to the deep southern model. By removing a handful of the deepest layers the model became numerically more stable and easier to manage. Also, the observed cooling rates of production wells could not be matched by placing the injection elements in layers depths corresponding to their drilled depths (Figure 5). Such a match could however be attained by pushing such injection elements much deeper in the model, as seen in Figure 6.

Inverse Calibration

With the model mesh described in the preceding section at hand and initial and boundary conditions set, the model work proceeded to the calibration phase. This intensive and time demanding endeavor proceeded with both forward and inverse model runs. Additionally, many new numerical modeling behaviors were encountered and handled during the course of the work.

The large volume of field data on Steamboat makes the numerical reservoir model ideal for automated calibration of the model parameters using tools like iTOUGH2. The inverse algorithm's central part is the objective function. The objective function measures the misfit between the data and the corresponding modeling result. The standard method used here is weighted least squares, i.e., the objective function to be minimized is the sum of the residuals weighted by the inverse of the measurement error. The mathematical expression is shown below. Here, S is the

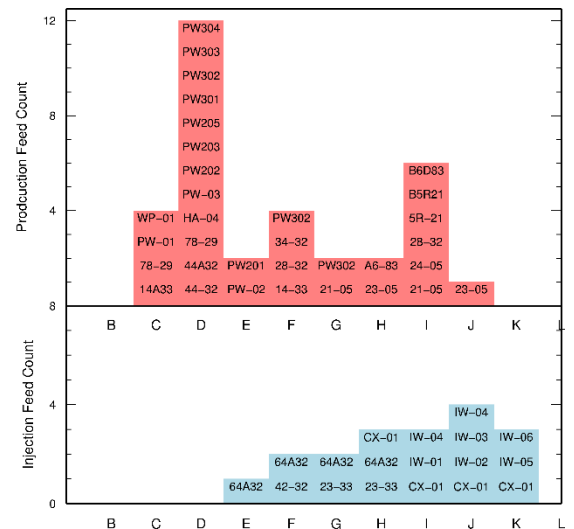


Figure 6. Steamboat wellfield feedzone count by model layers and their names.

objective function's numerical value, r_i is the difference between the observed and calculated system for observation number i , and σ_z is the standard deviation of a field measurement supplied to the inverse algorithm, valid for a number of observations belonging to group z .

$$S = \sum_{i=1}^m \frac{r_i^2}{\sigma_z^2}$$

Table 1 lists in more detail the data being imported to the inverse file of iTOUGH2. The total number of observations (m in above formula) is nearly 7000: 1200 in steady state temperature of wells, 1758 for transient enthalpy measurements of production wells, 155 in mass generation for well PW-1 on deliverability and finally about 3700 values for pressure drawdown in production and observation wells, largely coming from converting measured flow rates to drawdown using a factor of 100 kg/s/bar. The code is instructed to compare computed and observed values at 171 calibration times.

Table 1. Overview of data sets in the Steamboat model.

Property	Number
Number of datasets	1275
Number of calibration times	171
Number of parameters specified	22-80
Number of TOUGH-related parameters	22-80
Number of TOUGH-independent parameters	0
Number of inactive parameters	0
Number of tied parameters	0
Number of free parameters (n)	22
Number of parameters with prior info.	0
Number of regularization terms	0
Number of TEMPERATURE	1200
Number of ENTHALPY	1758
Number of MASS IN PLACE	170
Number of GENERATION RATE	155
Number of PRES. DRAWDOWN	3683
Total number of observations (m)	6966
Degree of freedom (m-n)	6944

Often when setting up a numerical model of the current size, the modelers encounter previously unknown but tricky behavior of the numerical simulator that can be attributed to various factors. The following three examples come to mind and their solution:

- The date feature of the iTOUGH2 inverse file is of fantastic help. This feature is actually based on earlier cooperation of Stefan Finsterle and the authors, incorporating the convenient date2sec and sec2date Fortran algorithms developed in the early 90s by Orkustofnun in Iceland (Árnason 1993).
- The very high permeability values of Steamboat led us to scrutinize the perturbation of model parameters used to compute the Jacobian matrix of the inverse algorithm. The value of 0.5 % was initially used, but had here to be raised to 2.5 % to correctly estimate the derivatives needed for the Jacobian matrix (>>> PERTURB: 2.5 %).
- Omit residual steam saturation in relative permeability curves. The authors have generally set 5% volumetric steam saturation as a threshold for the steam phase to become

mobile. This cosmetic but theoretically loyal definition leads to much higher number of iterations during the Steamboat model TOUGH2 time stepping than we found acceptable. Experimenting with the relative permeability function definition, making the steam phase mobile immediately upon flashing, greatly reduced the number of iterations and execution time.

Finally, the inverse calibration benefitted substantially from the steady-state-save feature of iTOUGH2. Thus, all data are calibrated against in the same forward run, both steady state and transient. The time management in iTOUGH2 also allowed for pressure and temperature data in newer Steamboat wells to be specified at the date of well completion instead of time zero in the model, here set at January 1, 1981.

Matching the Initial Pressure and Temperature Distribution

Figure 7 compares the early downhole pressure data to the steady state model pressure for wells 21-5 and IW-2 as a representation of the field. The current model is of unusual setup in the inverse file as a general assumption had to be made on pressure drawdown histories to calibrate against. The negligible pressure drawdown observed in Steamboat is due to the very high well productivity indices as well as good pressure support from the alluvium shallow strata with nearly 100% reinjection. A general field scale productivity index of 200 kg/s/bar, coming from downhole pump management, was used to estimate pressure drawdown in the model production and injection elements. The pressure loss is split between turbulent and Darcy flow. Thus a 100 kg/s/bar productivity index was used to compute pressure drawdown histories in all production wells. Furthermore, a standard deviation of 1 bar was assigned to each pressure drawdown dataset in the model inverse file to dampen these estimated data impacts on the iTOUGH2 objective function. Despite being experimental, this assumption proved to be very beneficial to the model calibration.

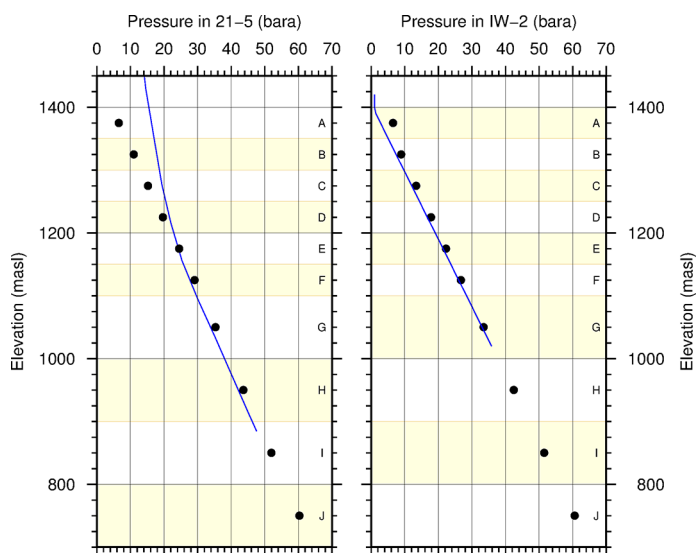


Figure 7. Steady state model (●) and field pressure in 21-5 (South) and IW-2 (North).

For example, it constrained some of the higher 1-10 Darcy model permeabilities being calibrated by the inverse process.

The model pressure is dictated by the pressure of the top inactive Layer A and by mass sinks to the north of Lower Steamboat. The pressure drawdown data discussed above is dictating the observation block of the inverse file and performed well in matching the measured data. Figure 7, therefore, is essentially reflecting the top layer pressure that served as the model pivot point depth. It also shows that the simulated model pressure is 2-4 bars higher than the measured data. This slight overpressure was deliberate due to otherwise slow model forward runs due to flashing in shallow elements. In the end, however, the steady state model pressure is well reflecting of the initial field pressure.

As discussed in Table 1, a sizeable number of datasets be-

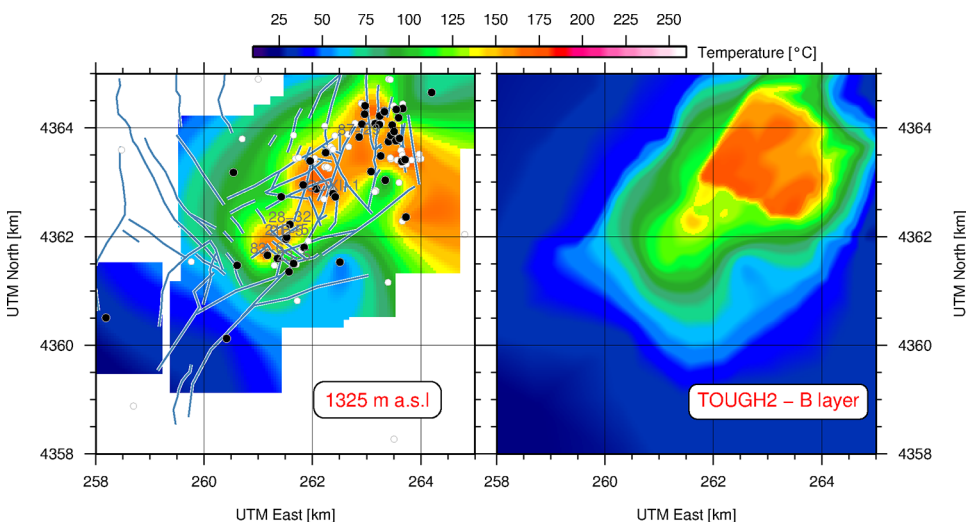


Figure 8. Natural state field and model temperature in layer B at 1325 m a.s.l.

came available in calibrating the present model. These are split between downhole observations and time transient wellhead flow and enthalpy histories. Each time the model was calibrated, a set of these graphics were generated, totaling to about 200 figures.

Figure 8 shows that in Layer B, the model natural state temperatures capture quite nicely the well data. Note, however, that the sharp south boundary of the Lower Steamboat anomaly coincides with the south boundary of the CrusB rocks and may have a smoother appearance in the real world.

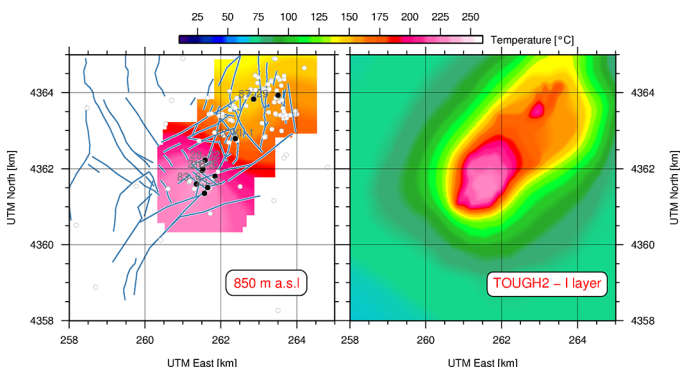


Figure 9. Natural state field and model temperature in layer I at 850 m a.s.l.

The model match to the natural state field temperature distribution continues to be fairly good down through the vertical extent of the model. A possible flaw is a larger extent of the model thermal anomaly to the east but again there are scarce field data here for matching the temperature. Isolated yellow dots in the red color area of both figures correspond to steam fumaroles used to cool the model locally.

The numerical model continues to show elliptical NNE trending temperature anomaly in Layer I, shown in Figure 9, while the field data is confined to only nine wells. The hot upflow zone under the Steamboat Hills is very apparent. The thermal anomaly extent is also beginning to shrink due to a local pressure low of the upflow area and a resulting horizontal boundary recharge from outer and colder model boundaries. This is necessary to capture the temperature reversal seen in many of the deeper wells.

Model Cooling in Years 2000 and 2012

The Steamboat resource management needs to account for the gentle cooling rates being observed. However, these cooling rates are also valuable data to calibrate and form one third of the data points comprising the objective misfit function being minimized by iTOUGH2.

Table 2 summarizes some of the cooling plot statistics, particularly that maximum cooling coincides with injection wells where the formation temperature was initially near 200 °C but has cooled due to the 100 °C water being injected directly to a well element. The cooling can also be an

artifact of cold water injectate sinking in fractures down to deeper and hotter model layers by gravity only. There are elements in model Layer D that had slight boiling prior to production from the model, and as production occurs, a large temperature increase is computed. However, this is just the result of two-phase mass and heat balance and should be overlooked. There are other elements that heat by 5-10 °C, likely attributed to fast water flow inside fractures, vertical or horizontal.

Table 2. Maximum temperature changes, ΔT (°C), for each model layer from 1981 to 2012.

Layer	Min	Max	Layer	Min	Max
B	-56	6	I	-75	9
C	-98	6	J	-73	10
D	-102	34	K	-81	1
E	-94	0	L	-75	2
F	-89	1	M	-53	2
G	-89	8	N	-5	0
H	-81	11			

Figure 10 shows cooling in the very permeable Layer B where no injection well is specified. The computed cooling therefore has to arrive by vertical flow from the layers either above or un-

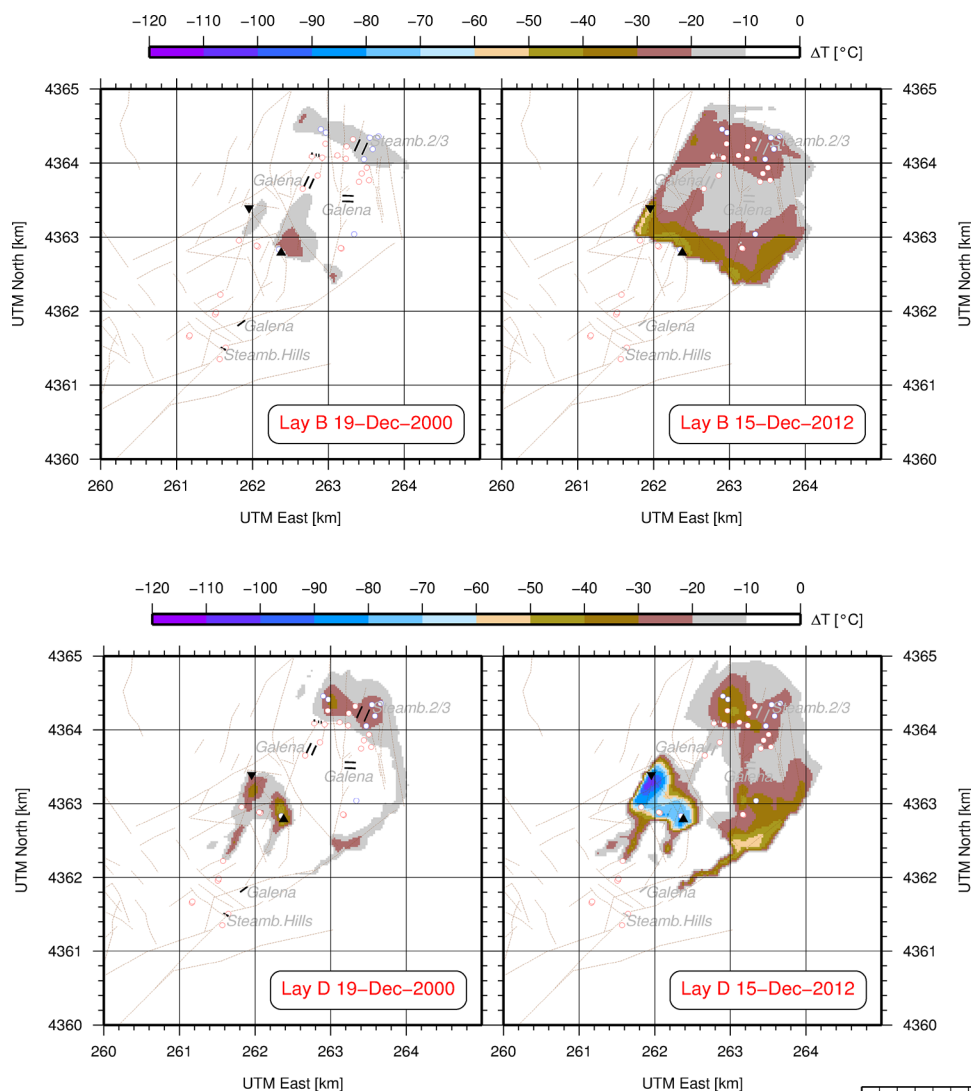


Figure 10. Cooling in layer B between 1981 and years 2000 and 2012, COXI-1 marked by black triangle and 42-32 marked by inverted black triangle.

derneath. Wells COXI-1 and 64A-32 are candidates for the cold water influx at the southern part of the cooling anomaly, again being very sharp due to the abrupt change in model permeability between the CrusB volume and the less permeable formation to the south of it (InneS). But generally the cooled water is efficiently sweeping heat out of the model layer, in good agreement with the high permeability estimated and the single porosity definition of this reservoir volume. Another model source of cooling is from the top layer A above, being able to recharge the model also vertically even at very moderate water table drawdown of only a few feet.

As noted before, it was virtually impossible to capture the slow cooling rates of wells tapping layers C, D and E by placing the injection points at their true depth inside these layers. The model cooling of layers C and D is therefore purely coming in by vertical convection as shown in Figure 11 (only Layer D is shown). Fracture permeability and upwelling fluid is to be suspected

Figure 11. Cooling in layer D between 1981 and years 2000 and 2012, COXI-1 marked by black triangle and 42-32 marked by inverted black triangle.

in the southern part of the figures while matrix recharge from below is a candidate for cooling of the Lower Steamboat area. Vertical cooling from the top Layer A is also a candidate for the midfield cooling, due to shrinking area of the grey shade color with depth. Wells 42-32 (inverted black triangle in Figures 10 and 11) and COXI-1/64A-32 (black triangle in Figures 10 and 11) are definitely generating their own cooling anomaly and the shape of the cooling area is clearly correlated to nearby fracture locations. Also, the Steamboat fault is sticking out as a cooling zone, channeling fluid from north to south.

Usable Heat from the Production Sectors

To simplify and integrate the multiple well performance histories into fewer graphs and curves, the Steamboat wellfield was split into five subsectors. Splitting was simply based on the N-coordinate of each well. Figure 12 shows the five numbered sectors, with wells in each area matching the corresponding font color of the number along the right side of the figure. Note that most wells are hosted in sector 5, while

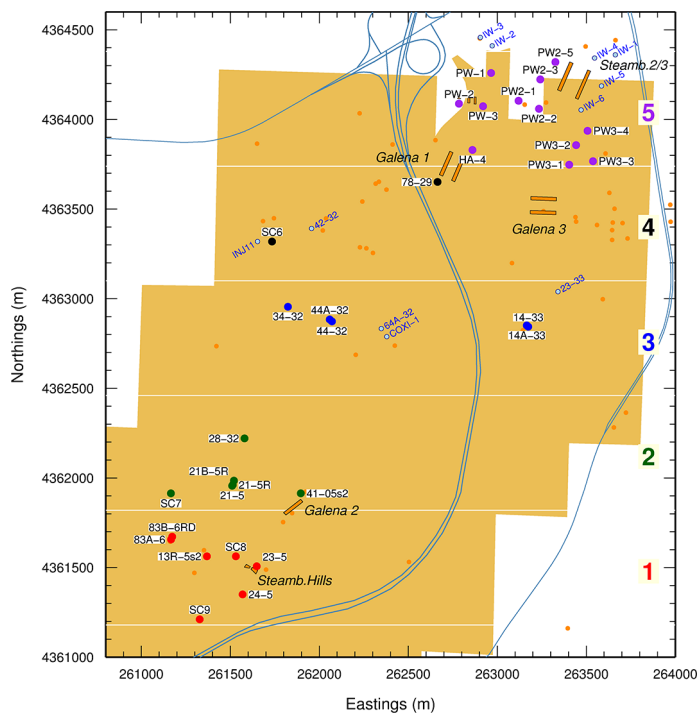


Figure 12. Power plants, production sectors (1-5), and production and injection wells.

sector 3 was virtually free of production wells up to about 2007. The production wells are shown with filled bullets and horizontal text label while the injection wells are shown with a light-blue dot and a diagonal text. The remaining idle wells are unlabeled but shown as orange dots.

It is of interest to study the cumulative heat flow out of Steamboat by using a production sector banding from north to south. Here the focus is on computed values only due to their convenient formatting in the iTOUGH2 output files. Results are shown in Figure 13. The average flowing enthalpy is highest under Steamboat Hills (sector 1) and lowest in Lower Steamboat (sector 5). An exception from this general behavior is the midfield sector 3, where the large injection wells COXI-1, 64A-32 and 23-33 are modeled with an overly strong cooling impact on the neighboring production wells 34-42, 44-32, 44A-32, 14-33 and 14A-33.

Also shown in Figure 13 is the usable heat (exergy) of produced mass, using boiling water temperature of 100 °C as rejection enthalpy (flow [kg/s] • (enthalpy-420) [kJ/kg]). This analysis shows that sector 5 was the primary workhorse for the past production sustaining about ¾ of the usable heat until late 2007. Then production begins from sector 3 and is simultaneously also gradually increased from sector 1. This change in management reduces the contribution of sector 5 to about 1/2 of the useable heat while the remainder is primarily coming from sectors 1 and 3.

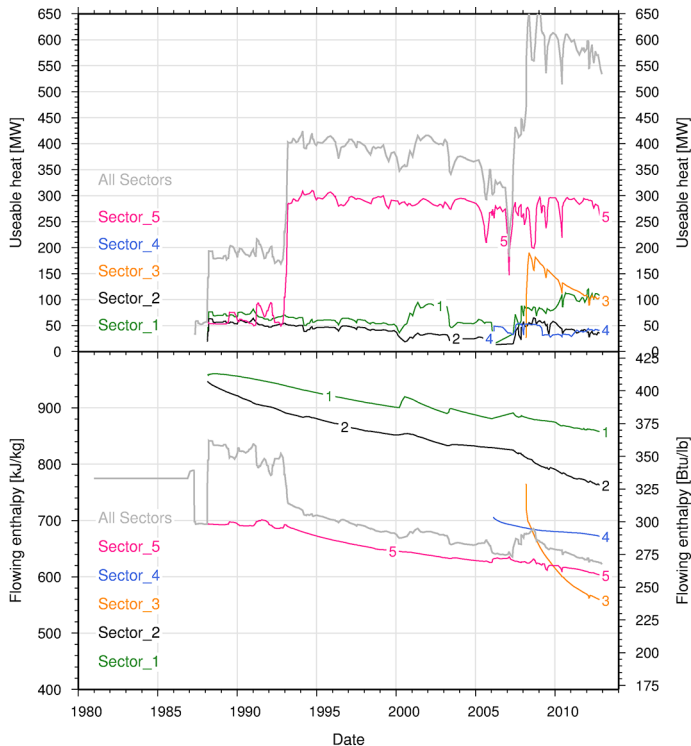


Figure 13. Mean enthalpy and usable heat by production sectors.

Figure 14 shows where heat has been removed from the model layers between 1981 and 2013. The heat extraction is very massive in the shallowest layers B-D and here certainly the existing heat in storage is being extracted. By going deeper into the model, the flow field is changing from matrix to fracture dominated. Heat sweep is

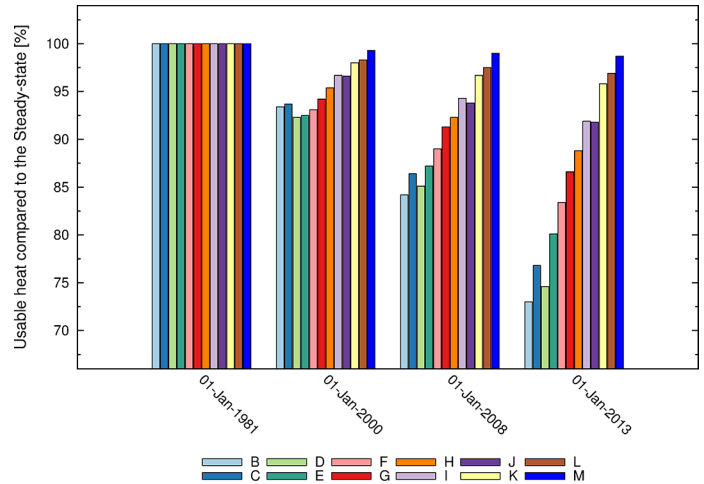


Figure 14. Useable heat by model layer and time.

therefore primarily by conduction between fault surfaces and the adjacent fairly tight rock matrix. The shortening of major faults at depth and heat recharge under Steamboat lead to progressively less heat removal as the layers get deeper, resulting in the stored heat in layer M virtually intact.

The analysis presented in Figure 14 can therefore be used as an argument for planning a field management strategy that combines optimized fluid flow management within the model major faults and additionally the drilling of new deep wells targeting sectors currently suffering little to moderate cooling.

Conclusions

The present numerical model of Steamboat proved to be a challenge, particularly in setting up a model mesh with the correct boundary and initial conditions needed to attain a satisfactory match between field and model data. One of the keys to successfully model the Steamboat reservoir was analyzing the conceptual reservoir model prior to setting up the numerical model mesh. The wells in Steamboat, despite being quite shallow, are tapping a large reservoir volume at greater depths. As a result, the initial model was made very thick to allow fluids to circulate to great depths. This assumption, however, proved to be too generous, forcing removal of the deepest 1 km of the model to end up with the layering shown in Figure 4. Additionally, the major vertical model faults were found to be sensitive for their lateral extent in the deepest model layers. Thirdly, the reservoir is best modeled as deep and fracture dominated resource under Steamboat Hills and shallow with effective matrix permeability under Lower Steamboat. Fourthly, the injection wells connected to the Lower Steamboat shallow matrix permeability seem to use this material only as a temporary lateral flow zone, prior to encountering vertically permeable structures. Structures, that in some cases appear to completely absorb the arriving injected water and divert it vertically to much greater depths. Only then does the injected fluid slow sufficiently to allow it to spread out and begin to follow the governing equations of groundwater flow used by the iTOUGH2 simulator.

The conceptual model was discretized into a first version of a numerical model mesh. The mesh was then calibrated until the

mesh was unable to match the field data. This led to a second loop of revising the conceptual model, the numerical model mesh, and a second calibration phase, a cycle that had to be repeated several times. Finally, after attaining a satisfactory match between field and model data, we realized that not only was the numerical model work used to match the large volume of field data at hand, but also in parallel the numerical model was used to improve the conceptual one. This is unusual at the scale of Steamboat, but when looking back, maybe this was the only option in updating the conceptual model other than drilling new deep wells. This project therefore not only generated a numerical model for Steamboat with future performance studies, but also it refined and detailed the reservoir conceptual model considerably.

References

- Arehart, G.B., M.F. Coolbaugh, and S.R. Poulson, 2003. "Evidence for a magmatic source of heat for the Steamboat Springs geothermal system using trace elements and gas geochemistry." *Geothermal Resources Council Transactions*, vol. 27, p. 269-274.
- Árnason, Þ., 1993. "Time-series analysis with sec2date and date2sec." Orkus-tofnun short report ÞA-93/01, 4 pp.
- Desormier, 1984. "Geologic Report on the Proposed Steamboat Springs Unit, Washoe County, Nevada." Phillips Petroleum Company, April, 1984, 31 pp.
- Finsterle, S., 2007. "iTOUGH2 User's Guide." Lawrence Berkeley National Laboratory Report LBNL-40040.
- Silberman, M.L., D.E. White, T.E.C. Keith, and R.D. Dockter, 1979. "Duration of hydrothermal activity at Steamboat Springs, Nevada, from spatially associated volcanic rocks." U.S. Geological Survey Professional Paper 458-D, 64 pp.
- Skalbeck, John, 2001. "Geochemical analysis and geophysical monitoring for hydrogeologic assessment of the Steamboat Hills and Southern Truckee Meadows area, Washoe County, Nevada." Washoe County Department of Water Resources, July 31, 2001.
- Skalbeck, J.D., Shevenell, L., Widmer, M., 2002. "Mixing of thermal and non-thermal waters in the Steamboat Hills area, Nevada, USA." *Geothermics*, vol. 31, p. 69-90.
- Spampanato, et al., 2010. "Overview of the Deep Geothermal Production at the Peppermill Resort." *Geothermal Resources Council Transactions*, vol. 34, p. 957-962.
- Thompson, G.A., and White, D.E., 1964. "Regional geology of the Steamboat Springs area, Washoe County, Nevada." U.S. Geological Survey Professional Paper 458-A, 52 pp.
- Walsh, et al., 2010. "High Angle Fracture-Controlled Permeability at Upper Steamboat Hills Geothermal Field, NV." *Geothermal Resources Council Transactions*, vol. 34, p. 833-837.
- Wessel, P., W.H.F. Smith, R. Scharroo, J.F. Luis, and F. Wobbe, 2013. "Generic Mapping Tools: Improved version released." *EOS Trans. AGU*, vol. 94, p. 409-410.
- White, D.E., 1968. "Hydrology, activity, and heat flow of the Steamboat Springs thermal system, Washoe County, Nevada." U.S. Geological Survey Professional Paper 458-C, 109 pp.
- White, D.E., G.A. Thompson, and C.H. Sandberg, 1964. "Rocks, structure, and geologic history of the Steamboat Springs thermal area, Washoe County, Nevada." U.S. Geological Survey Professional Paper 458-B, 63 pp.
- Yankee-Caithness Joint Venture, 2002. "A Structural interpretation and discussion of geologic controls on the distribution of the producing reservoir in the Steamboat Hills Area, Nevada." Internal Document, 33 pp.

